On the hydrodynamics of rocket propellant engine inducers and turbopumps

L d'Agostino

Civil and Industrial Engineering Department, Pisa University, Pisa 56122, Italy

E-mail: luca.dagostino@ing.unipi.it

Abstract. The lecture presents an overview of some recent results of the work carried out at Alta on the hydrodynamic design and rotordynamic fluid forces of cavitating turbopumps for liquid propellant feed systems of modern rocket engines. The reduced order models recently developed for preliminary geometric definition and noncavitating performance prediction of tapered-hub axial inducers and centrifugal turbopumps are illustrated. The experimental characterization of the rotordynamic forces acting on a whirling four-bladed, tapered-hub, variable-pitch high-head inducer, under different load and cavitation conditions is presented. Future perspectives of the work to be carried out at Alta in this area of research are briefly illustrated.

1. Introduction

Figure 1 illustrates the power/weight ratio of rocket propellant feed turbopumps used in the US Mercury, Gemini, Apollo and Space Shuttle propulsion systems from the early '60s to the '80s. The ten-fold increase of the power density clearly indicates that nowadays the criticalities of these machines are radically different from those of more conventional land or sea-based applications.

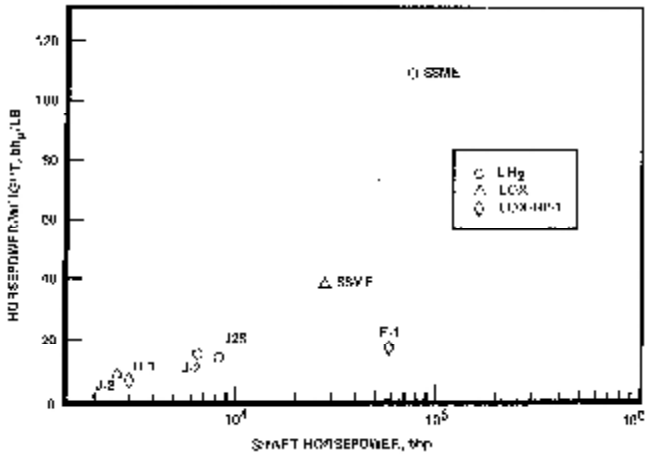

Figure 1. Power/weight evolution of propellant feed turbopumps for US space rocket engines (Rockwell International, personal communication).

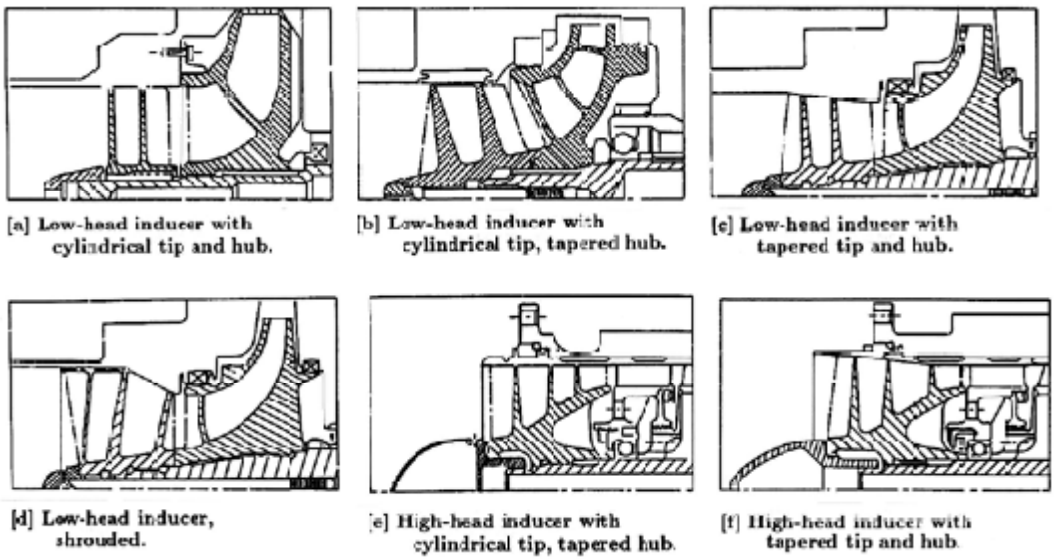

Figure 2. Typical geometries of cavitating inducers (from [22] Jakobsen 1971).

Inducers are often employed in today's rocket propellant feed turbopumps upstream of the centrifugal stage in order to improve the suction performance and reduce the propellant tank pressure and weight. Since their first introduction in space propulsion applications, the typical geometry of inducers has evolved as illustrated in **Figure 2**, taken from [22] Jakobsen 1971. Earlier low-head inducers were essentially axial flow impellers with constant-pitch helical blading and nearly uniform mean radius, mostly relying on the blade lift for raising the fluid pressure. Instead, today's high-head inducers are mixed-flow machines with tapered hubs, nearly cylindrical casings and variable-pitch blades, where a significant portion of the pressure rise is generated by the work developed by centrifugal forces in combination with the radial displacement of the fluid through the impeller. Compared to centrifugal pump impellers, inducers have fewer blades (usually 3 or 4) with smaller angles of attack, larger stagger angles (70 to 85 deg) and significantly higher solidities (between 1.5 and 2.5), in order to distribute the fluid loads on a wider surface and increase the suction performance by reducing the pressure drop on the blade suction side. The resulting configuration, leads to relatively low values of the hydraulic efficiency due to the higher incidence of viscous and turbulent losses in the blade passages.

The development of accurate, physically based and realistic 3D theoretical models capable of simultaneously predicting the geometry and performance of axial inducers and radial turbopumps is of particular interest to rocket engineers in order to rapidly provide indications for the preliminary design of the machine. A number of 2D reduced order models based on the traditional throughflow theory approximations, with empirical corrections for incidence, friction and deviation losses, have been proposed by Lakshminarayana 1982 [23], 1985 [24], Brennen 1994 [5], 1995 [6], and Bramanti et al. 2007 [4] for the prediction of the noncavitating performance of inducers and centrifugal turbopumps. None of these methods, however, is capable of provide any guidance in the choice of the impeller geometry, which must be assigned as a known input of the problem and can only be iteratively refined by trial and error.

High power/weight ratios in turbopumps are attained by running the impeller at the maximum allowable speed and lower shaft torque. Therefore, supercritical operation under cavitating conditions with lighter – but also more flexible – shafts is often tolerated in rocket propellant feed turbopumps. In general, cavitation represents the major source of degradation of the suction performance, efficiency, useful life and reliability of turbopumps ([33] Stripling and Acosta 1962). More specifically, in space propulsion applications cavitation can provide the flow compliance and excitation for triggering dangerous fluid mechanic and/or rotordynamic instabilities ([32] Sack and Nottage 1965, [25] Natanzon et al. 1974, [7] Brennen and Acosta 1973, [8] Brennen and Acosta 1976 [8], Ng and

Brennen 1978, [3] Braisted 1979, [19] d'Auria, d'Agostino and Brennen 1995, [11] d'Agostino, d'Auria and Brennen 1998, [12] d'Agostino and Venturini-Autieri 2002, [13] d'Agostino and Venturini-Autieri 2003), or even, through the coupling with thrust generation, of the entire space vehicle (POGO auto-oscillations, [31] Rubin 1966).

The most critical rotordynamic instability in high performance turbopumps is the development of self-sustained lateral motions (whirl) of the impeller under the action of destabilizing forces of mechanical and fluid dynamic origin ([20] Ehrich and Childs 1984). The role of rotordynamic fluid forces in promoting rotordynamic instabilities by significantly modifying, in conjunction with cavitation, the dynamic properties of the impeller, and therefore the critical speeds of the whole machine, has long been recognized ([30] Rosenmann 1965). However, because of their complexity and the experimental difficulties in their measurement, so far rotordynamic fluid forces in cavitating inducers and turbopumps have received relatively little attention in the open literature ([21] Franz 1989, [1] Bhattacharyya 1994, [2] Bhattacharyya et al. 1997, [19] d'Auria, d'Agostino and Brennen 1995, [11] d'Agostino, d'Auria and Brennen 1998, [12] d'Agostino and Venturini-Autieri 2002, [13] d'Agostino and Venturini-Autieri 2003).

2. On the Hydrodynamic Design of High-Head Inducers

A useful and powerful tool for the performance definition and preliminary design of axial inducers for space rocket applications is represented by the fully 3D reduced order model recently developed at Alta (d'Agostino et al 2008a [14], 2008b [15]). Under the assumptions of incompressible, inviscid and irrotational flow, the model approximates the 3D flow field inside the blade channels by superposing a 2D cross-sectional vorticity correction to a fully guided axisymmetric flow with radially uniform axial velocity (see **Figure 3**). Suitable redefinition of the diffusion factor to bladings with non-negligible radial flow allows for integral control of the blade loading and for the estimate of the boundary layer blockage at the specified design flow coefficient, providing a simple way to better match the hub profile with the axial variation of the blade angle in variable-pitch tapered inducers. Carter's rule is used to account for flow deviation at the inducer trailing edge. Mass continuity, angular momentum conservation and the Euler equation are used to propagate the solution downstream and derive a simple 2nd order boundary value problem, whose numerical solution determines the steady, axisymmetric, axial flow at the inducer discharge. Finally, the noncavitating pumping performance is obtained by correcting the Euler head by means of suitable correlations for turbulence losses, flow incidence and deviation.

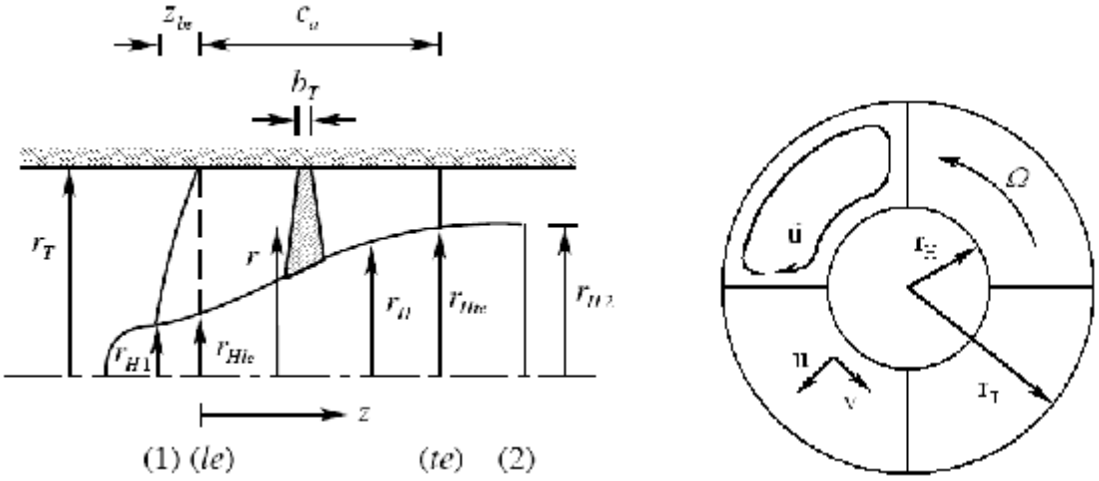

Figure 3. Schematic meridional cross-section of the inducer and nomenclature (left). 2D slip velocity correction in a generic axial cross-section of the inducer blade channels (right).

The model allows for the simultaneous definition of the impeller geometry and the prediction of its noncavitating performance based on a limited number of free parameters. It has been used for

effectively and rapidly designing a number of inducers with different characteristics (3-bladed and 4-bladed high-head inducers with tapered-hub and variable-pitch), which have been tested in Alta's facilities ([37] Torre et al 2011, [10] Cervone et al. 2011, [28] Pasini et al. 2011). As an example, **Figure 4** illustrates the geometrical and operational parameters of the DAPAMITO3 inducer designed by means of the above model.

Design flow coefficient	[--]	F_D	0.059
Number of blades	[--]	N	3
Tip radius	mm	r_T	81.0
Inlet tip blade angle	deg	g_{Tle}	83.10
Inlet hub radius (fully-developed blade)	mm	r_{Hle}	44.5
Outlet hub radius	mm	r_{Hte}	58.5
Mean blade height	mm	h_m	29.5
Axial length (fully-developed blade)	mm	c_a	63.5
Rotational speed	rpm	W	3000
Inlet hub radius	mm	r_{H1}	35.0
Axial length	mm	L	90.0
Diffusion factor	[--]	D	0.39
Tip incidence to blade angle ratio	[--]		0.3
Tip solidity	[--]	s_T	2.03
Incidence tip angle @ design	deg	a	2.07
Outlet tip blade angle	deg	g_{Tte}	74.58

Figure 4. Geometrical and operational parameters of the DAPAMITO3 inducer.

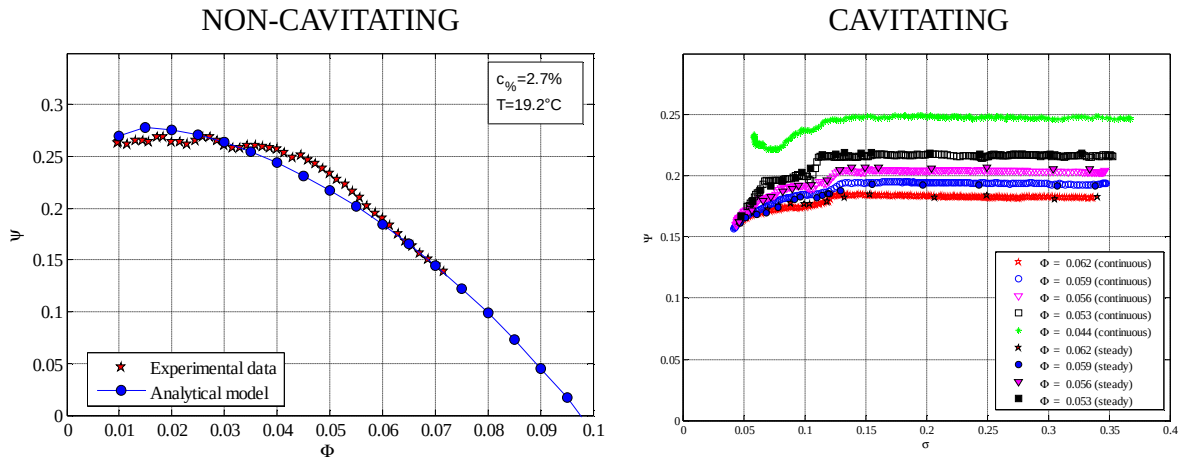

Figure 5. Comparison between the experimental and analytically predicted non-cavitating performance of the DAPAMITO3 inducer (left). The measured suction performance of the same inducer (right) at Ω = 2500 rpm and Re = 3.32 $\cdot 10^6$ (based on the tip speed and diameter) is also shown on the right.

The model has been successfully validated by comparing its results with the experimental data obtained at Alta for some space rocket inducers of European design and with the reported performance of a number of inducers tested in Japanese laboratories ([34] Torre et al. 2009, [14] d'Agostino et al. 2008a, [15] d'Agostino et al. 2008b). **Figure 5** illustrates the comparison between the non-cavitating performance predicted by the model for the DAPAMITO3 inducer shown in **Figure 4** and the experimental results obtained in Alta's Cavitating Pump Rotordynamic Test Facility for operation in water at room temperature and Reynolds number equal to about $3.32 \cdot 10^6$ based on the tip speed and diameter.

3. On the Hydrodynamic Design of Centrifugal Pumps

In 2011 d'Agostino et al., [17], [18], proposed a natural extension of the above model under more general assumptions, suitable for application to centrifugal pumps (see **Figure 6**, on the left). The model expresses the 3D ideal flow through helical blades with slow pitch and backsweep variations in the axial direction by superposing a 2D axial vorticity correction to a fully-guided forced-vortex flow with axisymmetric stagnation velocity in the meridional plane (see **Figure 6**, on the right). Also in this case the incompressibility and irrotationaly conditions for the impeller flow yield a set of constraints for the axial evolution of the blade pitch and backsweep that allows for the closed form derivation and complete definition of the impeller geometry and flowfield in terms of a reduced number of controlling parameters. In turn, mass and momentum conservation are used to account for the mixing of the flow leaving the impeller and its coupling with the 2D reduced order model of the flow in the diffuser. Next, similar considerations are used to match the discharge flow from the diffuser to the 1D model of the flow in the volute. Finally, the ideal noncavitating performance of the pump is computed by means of the Euler equation.

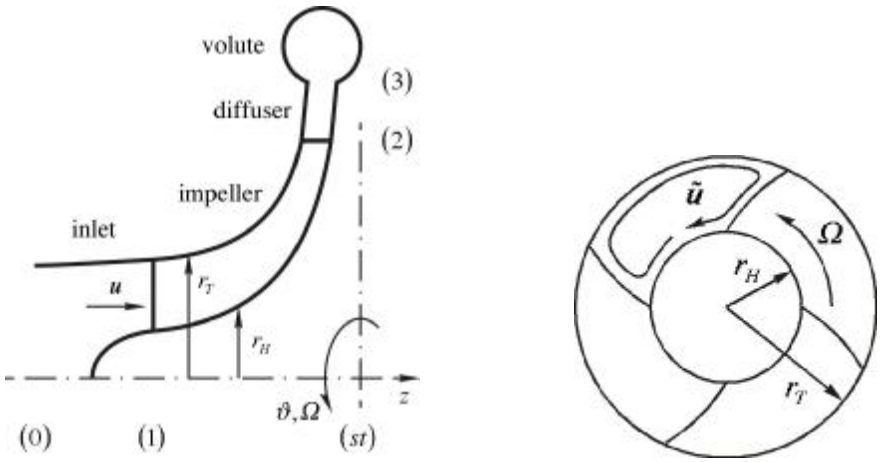

Figure 6. Schematic meridional cross-section of the pump and nomenclature (left). 2D slip velocity correction in a generic axial cross-section of the impeller blade channels (right).

Mixing and secondary flow losses are therefore already accounted for in this approach. However, the evaluation of the other main sources of losses and their dependence on the geometry of the flow path are also necessary for realistic prediction of the noncavitating performance of the machine and its dependence on the geometry of the flow path. The major contributions to these losses typically arise from flow incidence and mixing at the leading edges of the impeller blades and at the tongue of the volute, as well as from viscous effects in the blade channels ([18] d'Agostino et al. 2012). The above ideal flow model has therefore been interfaced with the calculation of the 2D axisymmetric turbulent boundary layers inside the blade channels, with the aim of developing an effective tool for rapid parametric optimization of the machine geometry and performance satisfying given requirements and/or constraints (see **Figure 7**).

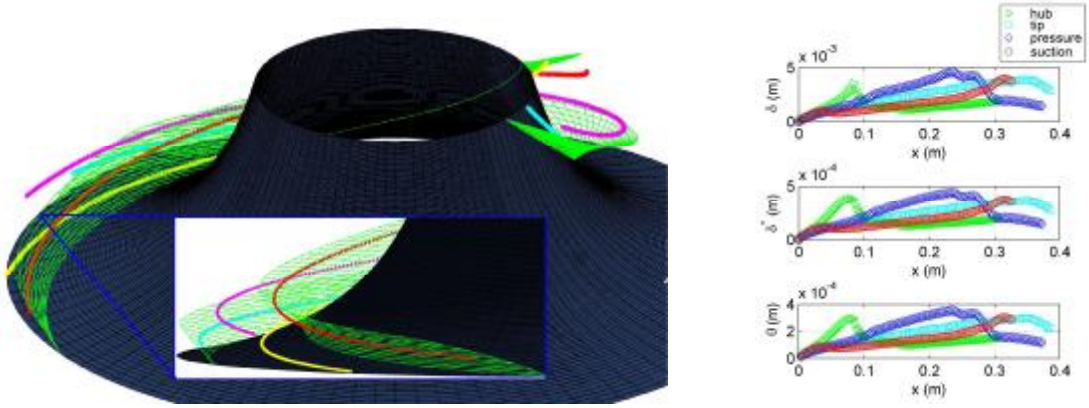

Figure 7. Streamlines of the boundary layers developing on the sides of the blade channels (left) and their nominal, displacement and momentum thicknesses (right).

The application of the model at design flow conditions determines the nominal head of the pump. In particular, with these results the design values of the non-dimensional parameters (F, Y, h, W_S and r_S) are determined as functions of the machine geometry, the tip incidence angle, the nature of the working fluid and a relatively small number of free controlling parameters. The computational efficiency of the model can then be exploited for varying the set of free parameters in order to optimize the design of the centrifugal pump under the assigned requirements and relevant constraints.

			VAMPIRE
Design flow coefficient	[--]	Φ_2	0.092
Number of blades	[--]	N	6.00
Outlet radius	mm	r_2	105.00
Inlet Tip radius	mm	r_{T1}	57.20
Inlet hub radius	mm	r_{H1}	31.80
Axial length (fully-developed blade)	mm	z_{H2}	46.40
Inlet tip blade angle	deg	γ_{T1}	56.60
Inlet backsweep angle	deg	c_1	0.00
Diffuser outlet radius	mm	r_3	126.00
Rotational Speed	[rpm]	W	1500.00
Design volumetric flowrate	[l]	V_{des}	0.02
Tip solidity	[--]	σ_T	2.26
Incidence tip angle @ design	deg	α	17.40
Outlet tip blade mean angle	deg	γ_{T2}	67.78
Outlet tip backsweep angle	deg	c_2	66.00
Exit blade height	mm	b_2	10.50
Exit cross-section volute radius	mm	R_4	38.20
Volute maximum radial dimension	mm	r_{V4}	201.50

Figure 8. Geometrical and operational parameters of the VAMPIRE pump.

This procedure has recently been exploited to design a radial machine, named VAMPIRE, with geometric characteristics and nondimensional performance similar to those typically used in rocket engine applications (see **Figure 8**). The pump, manufactured in 7075-T6 aluminum alloy, comprises a six-bladed unshrouded impeller, a vaneless diffuser and a single-spiral volute. At design conditions its predicted head coefficient and static-to-static hydraulic efficiency are 0.31 and 83%, respectively.

Radially straight blade leading edges have been chosen in this particular case, but more complex shapes are equally possible. As shown in **Figure 8**, downstream of the leading edges the model generates blade profiles with double and opposite curvatures. This blade shape combines the hydrodynamic advantages of realizing the nominal flow through the machine with superior structural stiffness and flutter resistance with respect to more conventional blade designs with straight cross-sections. The design of the machine has been completed with the sizing of the vaneless diffuser section and the single spiral volute for the extraction of the discharge flow.

The VAMPIRE pump has been tested by determining its pumping and suction performance in a number of experiments ([38] Valentini et al. 2013) in Alta's Cavitating Pump Rotordynamic Test Facility (CPRTF). Some typical results of these tests are shown in **Figure 9**. The measured pumping characteristic (darker dots in **Figure 9**) proved to be in excellent agreement with the model predictions (lighter dots in the same figure). The results confirmed that the model is indeed capable of efficiently defining and parametrically optimizing the geometry of mixed-flow and centrifugal pumps and accurately predicting their noncavitating performance. Besides, the experimental determination of the pump's cavitation characteristic also proved to be fully consistent with the expected suction performance of comparable machines, confirming the capability of the proposed model to generate hydrodynamically efficient turbopump designs.

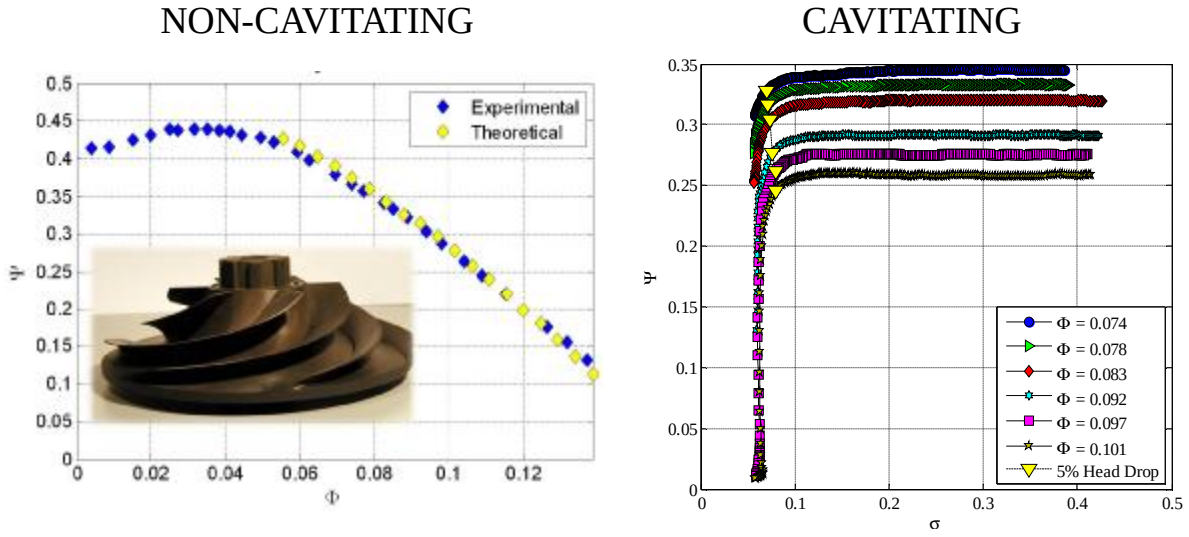

Figure 9. Comparison between the experimental and analytically predicted non-cavitating performance of the VAMPIRE pump at Ω = 1500 rpm and Re = 5.01 $\cdot 10^6$ (left). The measured suction performance of the same pump at Ω = 2300 rpm and T = 80 °C is also shown on the right for several values of the flow coefficient.

4. Rotordynamic Fluid Forces in Cavitating Inducers

The rotordynamic configuration of the Cavitating Pump Test Facility (CPTF) at Alta ([29] Rapposelli et al. 2002) has been specifically designed for the analysis of steady and unsteady fluid forces and moments acting on the impeller as a consequence of its whirl motion under cavitating or fully-wetted flow conditions, with special emphasis on the onset and development of lateral rotordynamic instabilities. It essentially consists in a closed, recirculating water loop with temperature, pressure, water quality, flow rate, rotation and eccentric whirl controls necessary for the pump to be tested under adjustable flux, load, speed, whirl and cavitation conditions.

The test item (inducer or pump) is mounted in a housing equipped with a rotating dynamometer for the measurement of the forces and moments acting on the impeller, as illustrated in **Figure 10**. The eccentricity of the test rotor with respect to the stator is generated by means of a double eccentric shaft mechanism. The two shafts are mounted one inside the other and their relative eccentricities can be vectorially combined before each rotordynamic test to finely adjust the resulting eccentricity of the

rotor in the range between 0 and 2 mm. The whirl motion of the test impeller is generated by an auxiliary motor driving the external shaft, while the impeller rotation is imparted by connecting the internal shaft to the main motor with an omokinetic coupling.

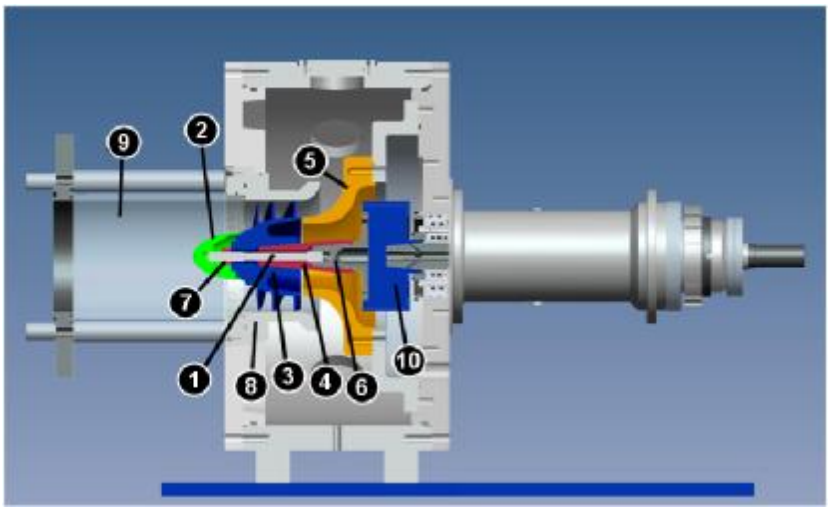

Figure 10. Rendering of the CPRTF test chamber assembly and its major components: (1) and (7) inducer fastening bolt, (2) inducer ogive, (3) inducer, (4) and (6) reference pins, (5) diffuser, (8) inducer casing, (9) transparent inlet duct, (10) rotating dynamometer.

The rotating dynamometer (part 10 in **Figure 10**) consists of two flanges connected by four posts of square cross-section acting as flexible elements and is mounted between the inducer and the driving shaft. The deformations of the posts are measured by 40 semiconductor strain gauges arranged in 10 full Wheatstone bridges, which provide redundant measurements of the instantaneous forces and moments acting on the impeller.

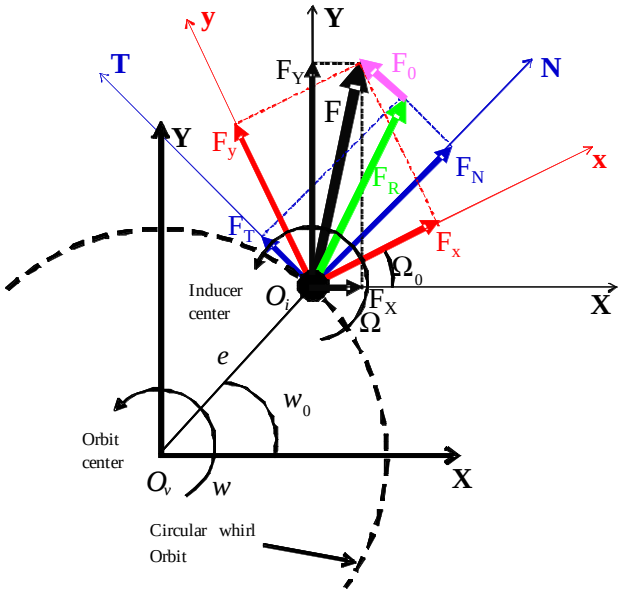

Figure 11. Rotordynamic forces in the laboratory and rotating reference frames.

Each bridge is temperature self-compensated up to 120 °C, with separate bipolar excitation and read-out for better reduction of cross-talking. The design of the sensing posts has been carried out as the result of a trade-off between acceptable sensitivity and sufficient structural resistance, operational stability and position control (stiffness) for the expected inertial characteristics of the suspended rotors.

Since the dynamometer is sensitive to the total force acting on the test rotor, the stationary force components in the laboratory frame (gravity, buoyancy and steady fluid forces) and the rotating centrifugal force generated by the whirl motion must be eliminated in the data reduction in order to isolate the rotordynamic fluid force generated by the imposed eccentricity. To this purpose it is necessary to known at any time during the run the angular orientations of the rotor and of the eccentricity using two optical pick-ups on the main and auxiliary motors. Finally, the normal and tangential components of the rotordynamic force along the directions of the eccentricity and its rotation are respectively evaluated, as indicated in **Figure 11**.

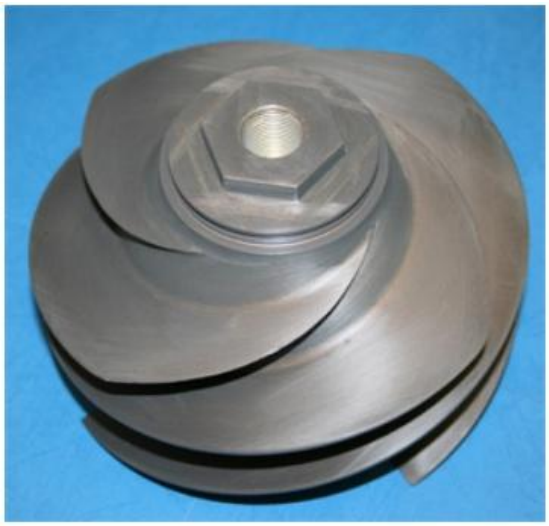

Design flow coefficient	[--]	Φ_D	0.070
Number of blades	[--]	N	4
Tip radius	mm	r_T	81.0
Inlet tip blade angle	deg	γ_{Tle}	81.10
Inlet hub radius (fully-developed blade)	mm	r_{Hle}	48.0
Outlet hub radius	mm	r_{Hte}	58.5
Mean blade height	mm	h_m	27.75
Axial length (fully-developed blade)	mm	c_a	63.5
Rotational speed	rpm	Ω	3000
Inlet hub radius	mm	r_{HI}	35.0
Axial length	mm	L	90.0
Diffusion factor	[--]	D	0.38
Ratio tip incidence / blade angle	[--]	α/β_b	0.3
Tip solidity	[--]	σ_T	2.25
Incidence tip angle @ design	deg	α	2.31
Outlet tip blade angle	deg	γ_{Tte}	72.46

Figure 12. The DAPAMITO4 inducer and its main characteristics.

Recent experiments carried out at Alta on a three-bladed and a four-bladed inducer have aimed at investigating the influence of cavitation on rotordynamic forces by means of tests where the impeller is subject to a whirl motion of given constant eccentricity and angular velocity ([35] Torre et al. 2010, [27] Pasini et al. 2010). A second set of experiments has also been conducted by means of a novel testing procedure capable of measuring the continuous spectrum of the rotordynamic force as a function of the whirl/rotating speed ratio ([36] Torre et al. 2011).

Typical results are shown in **Figure 13**, where the rotordynamic fluid force components acting on the four-bladed cavitating inducer illustrated in **Figure 12** (and indicated as DAPAMITO4) are plotted as functions of the ratio between the whirl and rotational speeds of the impeller (whirl ratio). In selecting the combination of rotor eccentricity and rotational speed to be used for a specific test impeller a suitable compromise must be drawn between the generation of measurable – and yet linear – rotordynamic forces and the limitations imposed by the lateral stability and structural integrity of the rotating dynamometer. In present tests on the DAPAMITO4 inducer the rotational speed is W=1750 rpm, the whirl eccentricity is e = 1.130 mm, the flow coefficient is F = 0.044 and the cavitation number is about s = 0.09. The selected values of the flow coefficient and cavitation number correspond to operation below the design flux (F = 0.059) under developed blade cavitation at 11% head degradation (i.e., close to breakdown conditions). Data corresponding to two different water temperatures (about 20 and 50 °C) are presented in order to investigate the (here negligible) influence of thermal cavitation effects. The close match with the results of tests carried at constant whirl speed (dots) effectively validates the procedure for the generation of the continuous spectra.

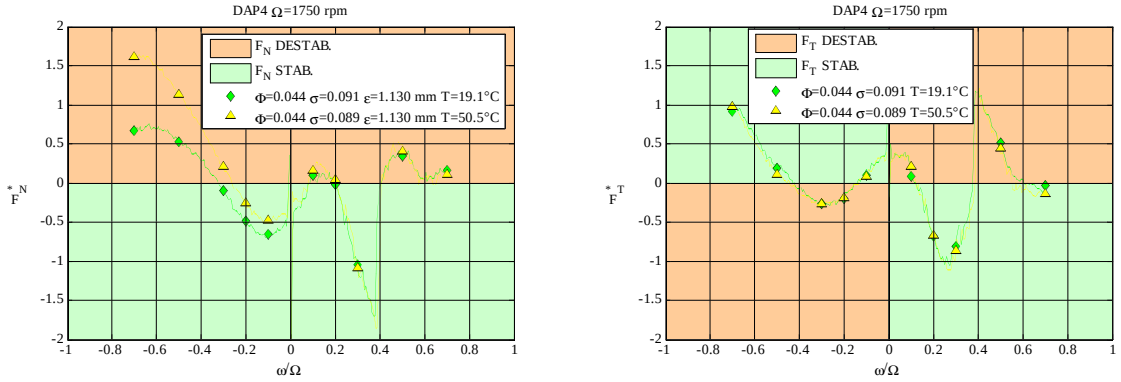

Figure 13. Normal (left) and tangential (right) components of the rotordynamic force on a four-bladed high-head inducer as a function of the whirl ratio, for F = 0.044, s = 0.089 and two different values of the water temperature. Regions shaded in green/red respectively correspond to stablizing/destabilizing components of the rotordynamic forces.

Under cavitating conditions, a well-defined destabilizing peak of the rotordynamic force has been systematically observed at a moderately positive value of the whirl ratio (w/W = 0.39). Similar findings have first been reported by Bhattacharyya 1994 [1] and Bhattacharyya et al. 1997 [2], who tentatively attributed the occurrence of this phenomenon to the interaction of the impeller with the backflow in the inlet duct. Flow visualization of backflow cavitation in present experiments allowed to confirm their intuition and clarify the physical mechanisms responsible for this phenomenon.

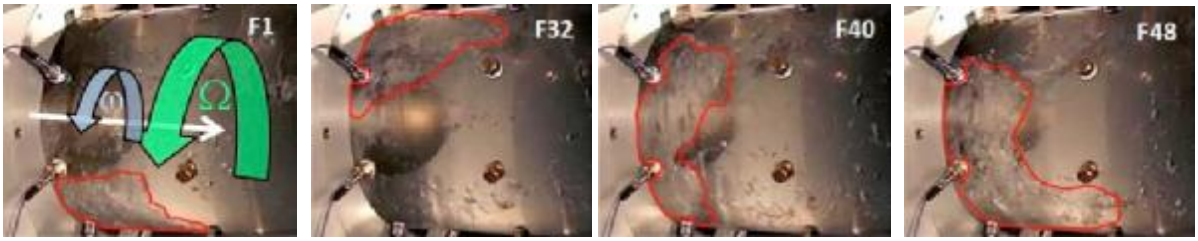

Figure 14. Frames extracted from a high-speed movie taken at 600 fps (w/W =0.39, F = 0.044, s = 0.089, T = 50.5 °C). Rotational and whirl speed vectors (first frame on the left), sequence of three frames (on the right) illustrating the passage of a concentrated cell of cavitation synchronously rotating with the whirl eccentricity.

Figure 15. Appearance of the cavitating regions at different values of the whirl ratio (F = 0.044, s = 0.089, T = 50.5 °C)..

Figure 14 shows a sequence of frames extracted from a high-speed movie recorded during the continuous hot test on the cavitating DAPAMITO4 inducer. The first frame indicates the coaxial

orientation of the rotational and whirl speed vectors, opposite to the approach flow direction to the inducer. The frames depict the test inducer at a whirl ratio corresponding to the destabilizing peak of the tangential rotordynamic force shown in **Figure 13** (w/W = 0.39). The cavitating region (highlighted by solid red lines) appears to be organized in a single well-defined structure rotating at the same angular speed of the whirl motion. The destabilizing force peak is observed when the force and the whirl eccentricity have opposite directions and appears to be associated with the reorganization of the cavitating regions into a single cell synchronously rotating with the whirl motion.

Conversely, as illustrated in **Figure 15**, at different values of the whirl ratio cavitation is broken into several regions, which can be associated to multiple backflow vortices. As a confirmation of these findings, previous experimental characterization of the flow instabilities on the same inducer has shown the onset of a rotating instability connected to backflow vortices at frequencies comparable to the whirl frequency for which the rotordynamic force peak has been detected in present experiments.

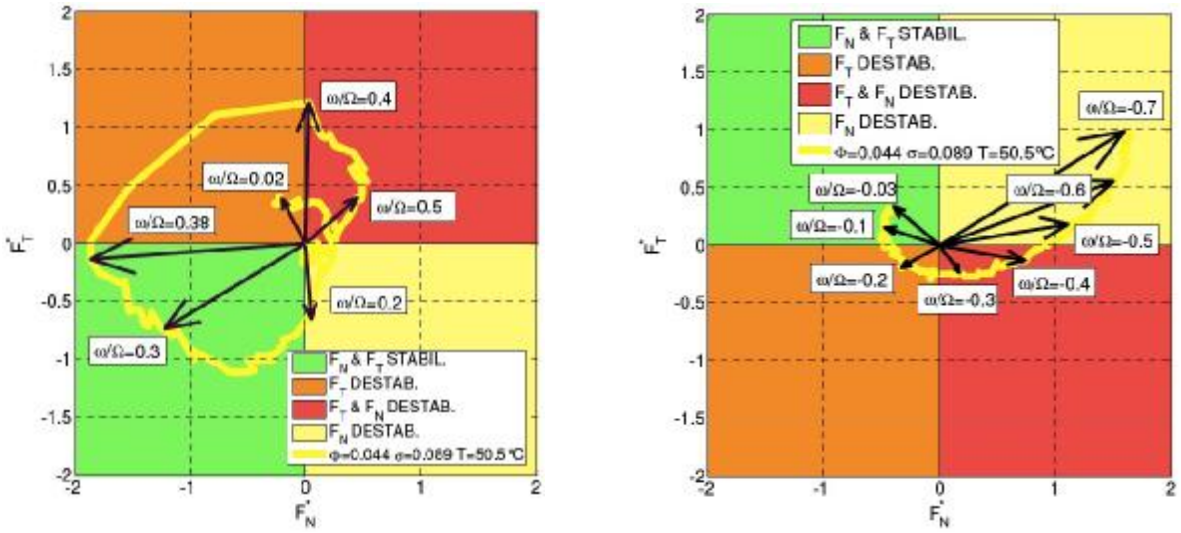

Figure 16. Rotordynamic force vector in the F_N*- F_T* plane for different positive (left) and negative (right) values of the whirl ratio under cavitating conditions (F = 0.044, s = 0.089, T = 50.5 °C).

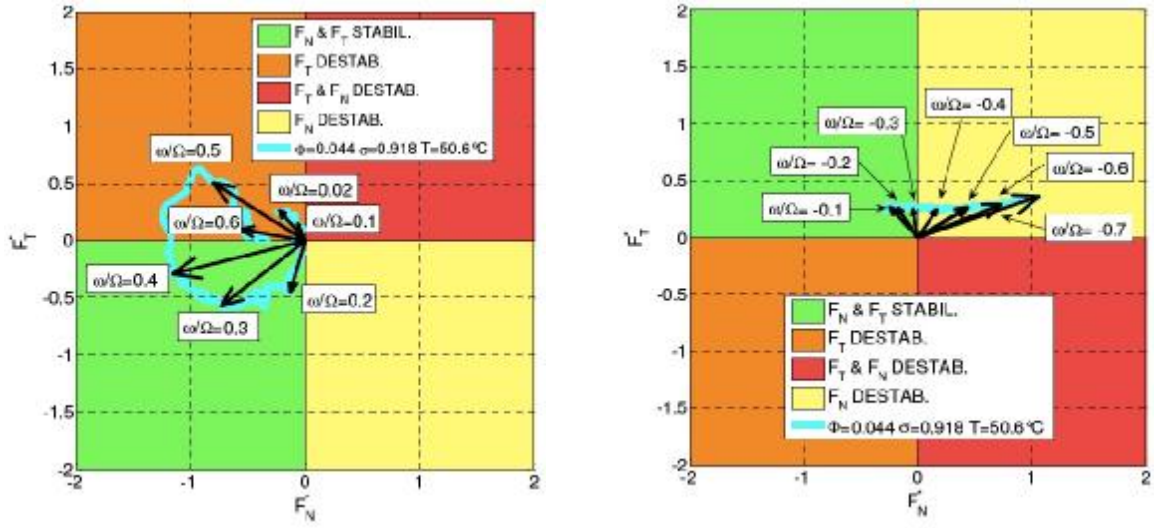

Figure 17. Rotordynamic force vector in the F_N*- F_T* plane for different positive (left) and negative (right) values of the whirl ratio under noncavitating conditions (F = 0.044, s = 0.918, T = 50.6 °C).

In **Figure 16** the rotordynamic forces of **Figure 13** are represented in both intensity and phase for different positive (left) and negative (right) values of the whirl ratio. It is worth noticing that the destabilizing force peak has the opposite direction of the whirl eccentricity. Furthermore, at the whirl ratio for which the peak is observed, a sudden transition between stabilizing (green) and strongly destabilizing (red) regions occurs.

Finally, for comparison **Figure 17** shows the same kind of charts for a noncavitating condition (F = 0.044, s = 0.918, T = 50.6 °C). In this case, the sudden transition from stabilizing to destabilizing conditions is not observed. At negative whirl ratios, the rotordynamic force shows a different behavior between cavitating and noncavitating conditions: not only the force intensity is higher when cavitation is present, but also its direction is completely different.

5. Dynamic Transfer Matrices of Cavitating Inducers and Turbopumps

The CPRTF has been recently upgraded in order to allow for the characterization of the dynamic behavior of cavitating inducers and turbopumps. In accordance with the indications of previous design analyses of the experiment ([9] Cervone et al. 2010), two configurations of the test loop are used (**Figure 18**), with different lengths (and impedances) of the discharge line, in order to generate at each oscillation frequency a set of four linearly independent measurements of the inlet/outlet flow fluctuations as required under cavitating conditions for the determination of the four elements H_{ij} of the dynamic transfer matrix:

$$\begin{bmatrix} \hat{p}_d \\ \hat{\dot{m}}_d \end{bmatrix} = \begin{bmatrix} H_{11} & H_{12} \\ H_{21} & H_{22} \end{bmatrix} \begin{bmatrix} \hat{p}_u \\ \hat{\dot{m}}_u \end{bmatrix}$$

relating the complex amplitudes of the pressure, $\hat{p}$, and mass flow rate, $\hat{\dot{m}}$, fluctuations of the upstream (u) and downstream (d) flow of the machine.

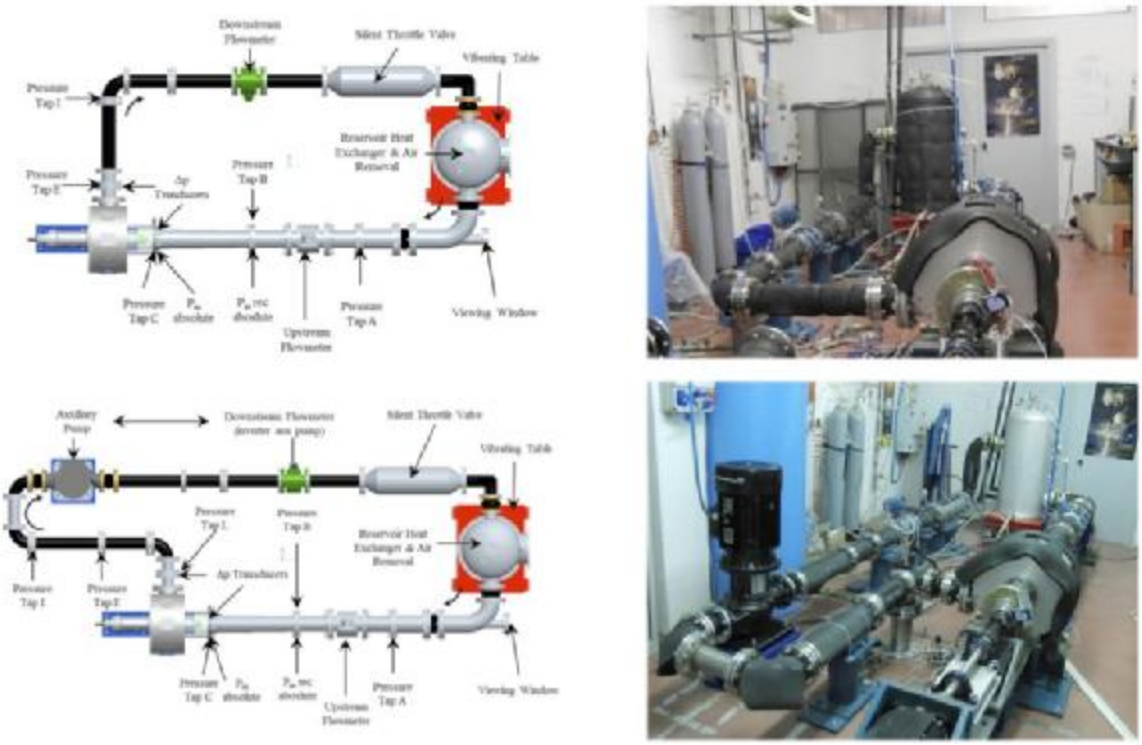

Figure 18. The “short” (top) and “long” (bottom) configurations of the test loop used for the experimental characterization of the dynamic transfer matrix of cavitating inducers and turbopumps.

The flow is harmonically excited with adjustable frequency and intensity by mounting on a vertical vibration table the free-surface tank, connected by flexible joints to the suction and discharge lines of the inducer (see **Figure 19**). A system of two synchronous counter-rotating electrical motors, with adjustable eccentricity and rotational speed, apply a vertical force to the tank with the desired intensity and frequency (up to 50 Hz). Piezoelectric pressure transducers have been located along the circuit at the stations indicated as "Pressure Tap" in **Figure 18**. The pressure oscillations at the inlet and outlet of the test chamber are measured directly, while the corresponding flow rate fluctuations have been deduced from the readings of the pressure difference on suitable sections of the inlet/outlet lines and the theoretical values of the relevant fluid dynamic impedances.

Direction of Vibration	Vertical
Maximum Vibration Frequency	50 Hz
Type of Electrical Motors	2 poles (2 motors)
Input Current	400 V, 3 phase
Input Power	4400 W (total)
Motors Eccentricity	0.5 mm (0÷30 Hz) 0.25 mm (30÷50 Hz)
Amplitude of Vibration	1 mm (0÷30 Hz) 0.5 mm (30÷50 Hz)
Maximum Load	500 kg
Supporting Plate Size	650 x 850 mm
Table Height	400 mm

Figure 19. The vibration table used in the CPRTF for exciting the flow with adjustable amplitude and frequency.

The measurement of flow rate fluctuations has traditionally been a crucial problem for the experimental characterization of the dynamic transfer function of cavitating turbopumps because of two main aspects:

- the very small relative intensity of the flow rate fluctuations, due to the modulation of an already relatively small volume of cavitation and to the relatively high value of the mean flow;
- the limited accuracy and frequency response of traditional flowmeters (electromagnetic, rotary, acoustic, optical, etc.), typically incompatible or just marginally compatible with the requirements of the present experimentation.

The determination of the flow rate fluctuations according to the above procedure successfully addresses both problems by relying for the measurements of pressure oscillations on extremely fast AC sensors, which are insensitive to the steady value of the flow rate and whose response becomes more intense at higher frequencies.

In synthesis, the procedure used to carry out of the dynamic characterization experiments is as follows:

- low pressure (0.2 bar) degassing of the water loop;
- attainment of the desired operational conditions (inducer rotating speed, flow rate, inlet pressure and temperature);
- excitation of the flow by electrically controlling the motion of the vibration table at the frequency of interest;
- acquisition of the pressure oscillations at different measurement stations along the test rig;
- reduction of the data for the evaluation of the components of the dynamic transfer matrix.

Figure 20 shows an example of the comparison between the amplitudes of the flow rate and pressure oscillations measured in exploratory experiments on the DAPAMITOR3 at $\Phi = 0.059$, $\sigma =$

0.177 and T = 20°C (on the left of the Figure) with the data obtained on impeller IV by Ng in the Pump Laboratory of the California Institute of Technology ([26] Ng 1976). All quantities are expressed as percentages of their means. The results confirm that the intensities of the flow fluctuations in both experiments are comparable. More specifically, the figure shows that pressure oscillations measured on the DAPAMITOR3 are slightly higher, most likely because of the higher efficiency of the vibration table used in Alta's experiments to excite the flow with respect to the flow rate fluctuator used at Caltech.

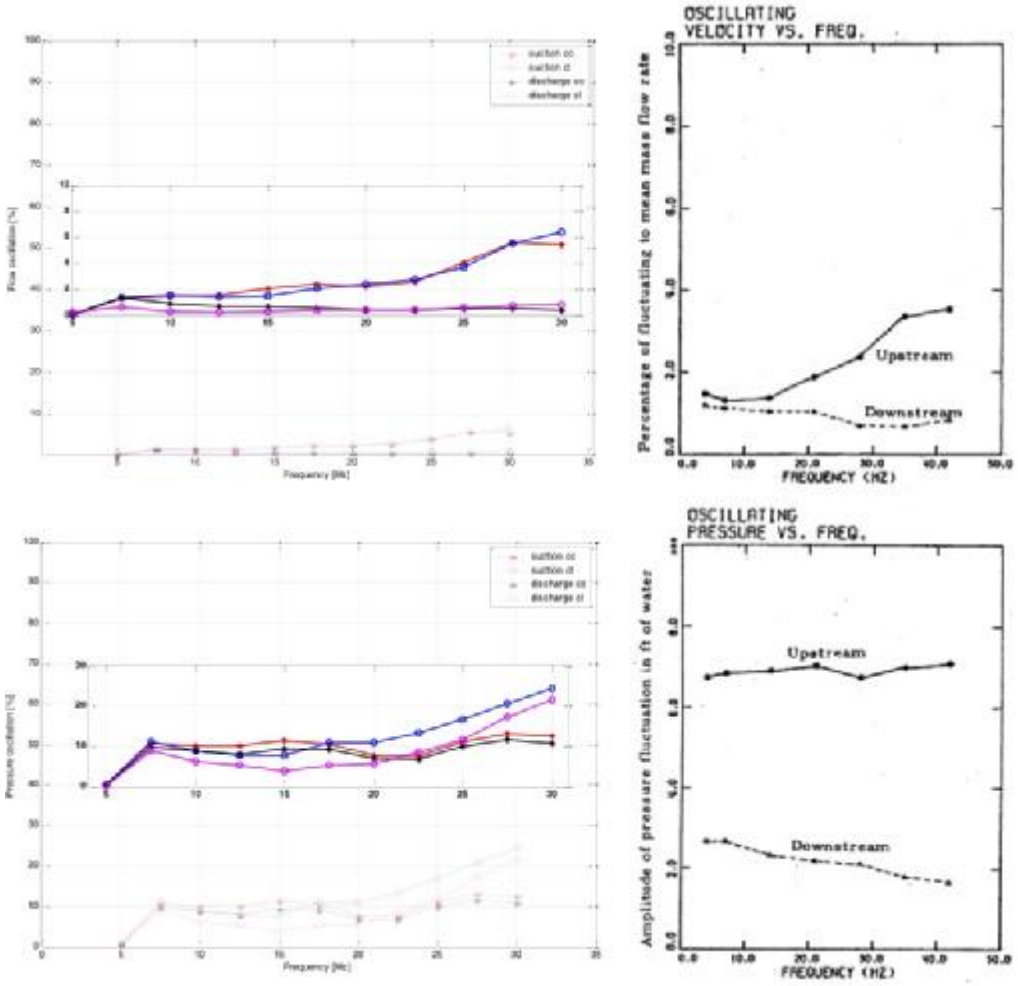

Figure 20. The amplitudes of the flow rate oscillations (top) and pressure oscillations (bottom) obtained during some of the dynamic characterization experiments of the DAPAMITOR3 inducer (same as the DAPAMITO3 but with rounded blade leading edge tips) at Alta (left) and of the impeller IV (right) at Caltech, [26] Ng 1976. The quantities are expressed as percentages of their mean values.

6. Conclusions

Based on the available evidence, the theoretical model developed at Alta proved to be able to provide accurate quantitative indications for geometry definition, 3D flow field description, characterization and control of the blade loading, and prediction of the noncavitating pumping characteristics of helical inducers with tapered hub and variable blade pitch angle. In the author's experience it therefore represents a useful tool for preliminary hydrodynamic design and performance analysis of high-head inducers for space propulsion applications.

The experimental results on the VAMPIRE pump in cold water tests conducted in the CPRFT confirmed that the reduced-order model recently developed at Alta for preliminary design of mixed-flow and centrifugal pumps is indeed capable of efficiently defining and refining the geometry of this class of machines and accurately predicting their noncavitating performance. On the other hand, the influence of the tip clearance on the noncavitating impeller performance has been euristically incorporated in the model and would benefit from more refined investigation. Finally, the suction performance tests on the VAMPIRE pump at design and off-design conditions are in line with the typical head degradation behavior of comparable machines for rocket propulsion applications. In particular, the results of hot and cold cavitating tests display the expected delay of breakdown conditions due to the thermal cavitation effects when the critical water temperature (here about 85 – 90 °C) for their occurrence is approached.

Under cavitating conditions, a destabilizing peak of the rotordynamic force on the tested inducer has been observed at positive subsynchronous whirl ratios. Optical observation of inducer backflow cavitation by high-speed video movies showed clearly indicated that the occurrence of this phenomenon, observed when the rotordynamic force and the whirl eccentricity have opposite directions, is due to the reorganization of backflow cavitating into a single well-defined cell, synchronously rotating with the whirl motion. Conversely, at different values of the whirl ratio, cavitation is broken into several regions that can be associated to backflow vortices. As a confirmation of these findings, a previous experimental characterization of the flow instabilities on the same inducer has shown the onset of a rotating instability connected to the backflow vortices at a frequency comparable to the whirl frequency at which the rotordynamic force peak has been detected.

Current advancement of the experimental evaluation of the dynamic transfer matrices of cavitating inducers and turbopumps successfully validated the novel technique used to force the flow and proved to be capable of effectively overcoming the accuracy and frequency response limitations of traditional flowmeters. Preliminary results obtained in the analysis of cavitating inducers are in line with the scant experimental data available in the open literature and confirmed the ill-conditioned nature of the dynamic characterization of cavitating turbomachines in forced forced-vibration experiments. Future work will be aimed at verifying the feasibility of experiments at different excitation frequencies on just one configuration of the test loop as a way to solve the present ill-conditioning problem and, in combination with maximum likelyhood estimate techniques, improve the quality of the results.

7. Nomenclature

7.1. Latin Symbols

c	blade chord
c_a	full-blade axial length
$\boldsymbol{F}$	force vector
F	force component
$\boldsymbol{F}^*$	nondimensional force vector
F^*	nondimensional force component
$\dot{m}$	mass flow rate
p	pressure
p^T	total pressure
r	radial coordinate
Re	Reynolds number, $\mathrm{Re} = 2Wr_T^2/n$
T	temperature
$\boldsymbol{u}$	velocity vector
u, v, w	radial, azimuthal and axial velocities
z	axial coordinate

7.2. Greek Symbols

a	blade incidence angle
g	blade angle
d	boundary layer nominal thickness
d^*	boundary layer displacement thickness
e	rotor eccentricity
h	hydraulic efficiency
J	azimuthal coordinate
q	boundary layer momentum thickness
m	Newtonian viscosity
n	kinematic viscosity
s	Euler number, $s = \left(p_u - p_V\right) \Big/ \frac{1}{2} r W^2 r_T^2$
F	flow coefficient, $F = \dot{m} \Big/ p r W r_T^3$
Y	head coefficient, $Y = \left(p_d^T - p_u^T\right) \Big/ r W^2 r_T^2$
w	whirl speed
W	angular speed
W_S	specific speed

7.3. Subscripts

d	downstream
D	design
T	tip
u	upstream
V	vapor

Acknowledgments

The author would like to acknowledge the invaluable contributions of the present and past members of the cavitation research group at Alta: Drs. Angelo Cervone, Lucio Torre and Angelo Pasini, doctoral students Giovanni Pace and Dario Valentini, as well as the help of the M.S. students who collaborated to various aspects of the work presented in this paper. The support of the European Space Agency under Contracts No. 20081/06/NL/IA, 4000102585/10/NL/Sfe and 22976/09/NL/S is gratefully acknowledged. The author would like to express their gratitude to Drs. Johan Steelant and Giorgio Saccoccia, ESA-ESTEC, Nordwijk, The Netherlands, for his constant attention and encouragement. Special thanks go to Dr. MacEukanoush of GMYS-Space.

References

[1] Bhattacharyya A 1994 *Internal Flows and Force Matrices in Axial Flow Inducers* (Pasadena: California Institute of Technology) Report No. E249.18

[2] Bhattacharyya A, Acosta A J, Brennen C E and Caughey T K 1997 *ASME Journal of Fluids Engineering* **199**(4) 768-74

[3] Braisted D M 1979 *Cavitation Induced Instabilities Associated with Turbomachines* (Pasadena: California Institute of Technology) Report No. E184.2

[4] Bramanti C, Cervone A and d'Agostino L 2007 A Simplified Analytical Model for Evaluating the Noncavitating Performance of Axial Inducers *43rd AIAA/ASME/SAE/ASEE Joint Propulsion Conference (Cincinnati, USA, 8-11 July 2007)*

[5] Brennen C E 1994 *Hydrodynamics of Pumps* (Oxford: Oxford University Press) Oxford

Engineering Science Series 44
[6] Brennen C E 1995 *Cavitation and Bubble Dynamics* (Oxford: Oxford University Press)
[7] Brennen C E and Acosta A J 1973 *J. of Spacecraft* **10**(3) 175-9
[8] Brennen C E and Acosta A J 1976 *ASME J. Fluids Eng*. **98** 182-91.
[9] Cervone A, Piccoli E A, Torre L, Pasini A and d'Agostino L 2010 Design of a Test Setup for the Characterization of the Dynamic Transfer Matrix of Cavitating Inducers *46th AIAA/ASME/SAE/ASEE Joint Propulsion Conference (Nashville, Tennessee, USA, 25-28 July 2010)*
[10] Cervone A, Torre L, Pasini A and d'Agostino L 2011 Cavitation and Flow Instabilities in a 4-Bladed Axial Inducer Designed by Means of a Reduced Order Analytical Model *47th AIAA/ASME/SAE/ASEE Joint Propulsion Conference (San Diego, California, USA, 31 July-3 August 2011)*
[11] d'Agostino L, d'Auria F and Brennen C E 1998 *ASME Journal of Fluids Engineering* **120** 698-704
[12] d'Agostino L and Venturini-Autieri M R 2002 Three-Dimensional Analysis of Rotordynamic Fluid Forces on Whirling and Cavitating Finite-Length Inducers *9th Int. Symp. on Transport Phenomena and Dynamics of Rotating Machinery (Honolulu, USA: 10-14 Feb 2002)*
[13] d'Agostino L and Venturini-Autieri M.R 2003 Rotordynamic Fluid Forces on Whirling and Cavitating Radial Impellers *CAV 2003, 5th International Symposium on Cavitation (Osaka, Japan, 11-14 Nov 2003)*
[14] d'Agostino L, Torre L, Pasini A and Cervone A 2008 A Reduced Order Model for Preliminary Design and Performance Prediction of Tapered Inducers *12th Int. Symp. on Transport Phenomena and Dynamics of Rotating Machinery (Honolulu, Hawaii, USA, February 17-22 2008)*
[15] d'Agostino L, Torre L, Pasini A and Cervone A 2008 *ASME Journal of Fluids Engineering* **130** (11)
[16] Torre L, Pasini A, Romeo L and d'Agostino L 2008 Firing Performance of Advanced Hydrogen Peroxide Catalytic Beds in a Monopropellant Thruster Prototype *44th AIAA/ASME/SAE/ASEE Joint Propulsion Conference & Exhibit (Hartford, USA, 21 - 23 July 2008)*
[17] d'Agostino L, Pasini A and Valentini D 2011 A Reduced Order Model for Preliminary Design and Performance Prediction of Radial Turbopumps *47th AIAA/ASME/SAE/ASEE Joint Propulsion Conference (San Diego, California, USA, 31 July-3 August 2011)*
[18] *d'Agostino L, Pasini A, Valentini D, Pace G, Torre L and Cervone A 2012 A Reduced Order* Model for Optimal Centrifugal Pump Design *(14th Int. Symp. on Transport Phenomena and Dynamics of Rotating Machinery, Honolulu, Hawaii, USA, 27 February–2 March 2012)*
[19] d'Auria F, d'Agostino L and Brennen C E 1995 Bubble Dynamic Effects on the Rotordynamic Forces in Cavitating Inducers *1995 ASME Fluids Engineering Summer Meeting (Hilton Island, South Carolina, USA, 13-18 August 1995)*
[20] Ehrich F and Childs S D 1984 *Mech. Engng.* **106** 66-79
[21] Franz R J 1989 *Experimental Investigation of the Effect of Cavitation on the Rotordynamic Forces on a Whirling Centrifugal Pump Impeller* (Pasadena: California Institute of Technology)
[22] Jakobsen J K 1971 *Liquid Rocket Engine Turbopump Inducers* (USA: NASA) NASA SP 8052
[23] Lakshminarayana B 1982 *ASME J. of Fluids Engineering* **104** 411-27
[24] Laskshminarayana B 1985 *Fluid Dynamics and Heat Transfer of Turbomachinery* (New York: Wiley) Chaps. 1-5
[25] Natanzon M S et al. 1974 *Fluid Mech. Soviet Res*. **3**(1) 38-45
[26] Ng S L 1976 *Dynamic Response of Cavitating Turbomachines* (Pasadena: California Institute of Technology)
[27] Pasini A, Torre L, Cervone A and d'Agostino L 2010 Rotordynamic Forces on a Four Bladed

Inducer *Proc. 46th AIAA/ASME/SAE/ASEE Joint Propulsion Conference (Nashville, USA, 25-28 July 2010)*

[28] Pasini A, Torre L, Cervone A and d'Agostino L 2011 Characterization of the Rotordynamic Forces on Tapered Axial Inducers by Means of a Rotating Dynamometer and High-Speed Movies *WIMRC 3rd International Cavitation Forum 2011 (University of Warwick, UK, 4-6 July 2011)*

[29] Rapposelli E, Cervone A and d'Agostino L 2002 A New Cavitating Pump Rotordynamic Test Facility *Proc.38th AIAA/ASME/SAE/ASEE Joint Propulsion Conference (Indianapolis, USA, 7-10 July 2002)*

[30] Rosenmann W 1965 Experimental Investigations of Hydrodynamically Induced Shaft Forces With a Three Bladed Inducer *Proc. ASME Symp. on Cavitation in Fluid Machinery (Chicago, USA, 7-11 Nov 1965)*

[31] Rubin S 1966 *J. Spacecraft and Rockets* **3**(8) 1188-95

[32] Sack L E and Nottage H B 1965 *ASME J. Basic Eng*. **87** 917-24

[33] Stripling L B and Acosta A J 1962 *ASME J. Basic Eng* **84** 326-38

[34] Torre L, Pasini A, Cervone A and d'Agostino L 2009 Experimental Performance of a Tapered Axial Inducer: Comparison with Analytical Predictions *45th AIAA/ASME/SAE/ASEE Joint Propulsion Conf. & Exhibit (Denver, Colorado, USA, 2-5 Aug 2009)*

[35] Torre L, Pasini A, Cervone A, Pecorari L, Milani A and d'Agostino L 2010 Rotordynamic Forces on a Three Bladed Inducer *Proc. Space Propulsion Conference (San Sebastian, Spain, 3-6 May 2010)*

[36] Torre L, Pasini A, Cervone A and d'Agostino L 2011 Continuous Spectrum of the Rotordynamic Forces on a Four Bladed Inducer *ASME/JSME/KSME 2011 Joint Fluids Engineering Conference (Hamamatsu, Japan, 24-29 July 2011)*

[37] Torre L, Pasini A, Cervone A, Pace G, Miloro P and d'Agostino L 2011 *AIAA Journal of Propulsion and Power* **27**(4) 890-8

[38] Valentini D, Pasini A, Pace G, Torre L and d'Agostino L 2013 Experimental Validation of a Reduced Order for Radial Turbopump Design *49th AIAA/ASME/SAE/ASEE Joint Propulsion Conference & Exhibit* (San Josè, California, USA, 15–17 July 2013)